Hall, Jonathan Michael MacGillivray; Leinweber, Derek Bruce; Young, Ross Daniel
Chiral extrapolations for nucleon magnetic moments
Physical Review. D. Particles, Fields, Gravitation and Cosmology, 2012; 85(9):094502:1-094502:8

http://dx.doi.org/10.1103/PhysRevD.85.094502

PHYSICAL REVIEW D **85,** 094502 (2012)

Chiral extrapolations for nucleon magnetic moments

J. M. M. Hall,[1] D. B. Leinweber,[1] and R. D. Young[1,2]

[1]*Special Research Centre for the Subatomic Structure of Matter (CSSM), School of Chemistry and Physics, University of Adelaide 5005, Australia*

[2]*ARC Centre of Excellence for Particle Physics at the Terascale, School of Chemistry and Physics, University of Adelaide 5005, Australia*

(Received 31 January 2012; published 3 May 2012)

Lattice QCD simulations have made significant progress in the calculation of nucleon electromagnetic form factors in the chiral regime in recent years. With simulation results achieving pion masses of order ~180 MeV, there is an apparent challenge as to how the physical regime is approached. By using contemporary methods in chiral effective field theory (χEFT), both the quark-mass and finite-volume dependence of the isovector nucleon magnetic moment are carefully examined. The extrapolation to the physical point yields a result that is compatible with experiment, albeit with a combined statistical and systematic uncertainty of $\pm 10\%$. The extrapolation shows a strong finite-volume dependence; lattice sizes of $L > 5$ fm must be used to simulate results within 2% of the infinite-volume result for the magnetic moment at the physical pion mass.

DOI: 10.1103/PhysRevD.85.094502 PACS numbers: 12.38.Gc, 12.38.Aw, 12.39.Fe, 13.40.Em

I. INTRODUCTION

The distribution of the electric and magnetic charge currents of the nucleon are characterized by the elastic electromagnetic form factors—for recent reviews on experimental progress, see Refs. [1–5]. The description of the electromagnetic form factors in terms of the elementary degrees of freedom of QCD has seen significant progress through recent advances in lattice QCD simulations [6–10].

Lattice QCD simulations of the electromagnetic form factors of the nucleon [11] are now probing into the chiral regime, where the QCDSF Collaboration have recently reported results at pion masses as low as ~180 MeV [10]. The results of this work have presented a challenge in the pion-mass extrapolation to the physical point. The results presented in Ref. [10] have been used to investigate the applicability of a range of chiral effective field theory (χEFT) methods, including ''heavy-baryon'' [12], ''small scale expansion'' [13], and ''covariant baryon'' approaches [14]. It has been demonstrated that there is a difficulty in achieving a consistent quantitative description of the pion-mass dependence of key observables (such as magnetic moments and charge radii) between the physical point and the lightest simulation results [10]. This issue has persisted across a number of simulations [15,16]. In the present manuscript, a chiral extrapolation of the QCDSF results is developed for the isovector nucleon magnetic moment based on finite-range regularized (FRR) χEFT [17,18].

In the application of FRR to the extrapolation of the magnetic moment, new developments are utilized in order to ensure the robustness of the extrapolation procedure. These include the identification of the preferred finite regularization scale directly from the lattice results [19] and a determination of an upper bound of the pion mass that can be reliably incorporated in the extrapolation [20]. A feature of the analysis is that the combination of both finite-volume corrections and the onset of rapid nonanalytic behavior in the chiral regime leads to an extrapolation that is compatible with the experimental value. The analysis provides the predicted quark-mass dependence for a range of fixed-volume lattices, which act to emphasize the importance of achieving large volumes in order to reveal the strong nonanalytic behavior directly on the lattice.

The lattice QCD results for the magnetic moment of the isovector nucleon, μ_N^{v}, from the QCDSF Collaboration are displayed in Fig. 1. The lattice calculation used $N_f = 2$ and the $\mathcal{O}(a)$-improved Wilson quark action [10]. The isovector combination $(p - n)$ is considered to avoid calculating the disconnected loops that occur in full QCD. To ensure that the lattice results give a reasonable approximation to the infinite-volume limit, the following restrictions are applied: $L > 1.5$ fm and $m_\pi L > 3$. There are nine lattice points that satisfy these criteria from the original set of results. The lattice sizes considered vary from 1.7 fm to 2.9 fm. A simple linear fit is included in this plot, which does not take into account the chiral loop integrals, nor the finite-volume corrections to the data. Neglecting these effects, it is not surprising that the linear trend does not reach the experimental value of the magnetic moment at the physical pion mass. The use of extended χEFT methods in performing the extrapolation to the physical point will now be explored.

II. CHIRAL EFFECTIVE FIELD THEORY

The elastic matrix element for the baryon-photon interaction can be parametrized by the Dirac and Pauli form factors, F_1 and F_2, respectively, written as

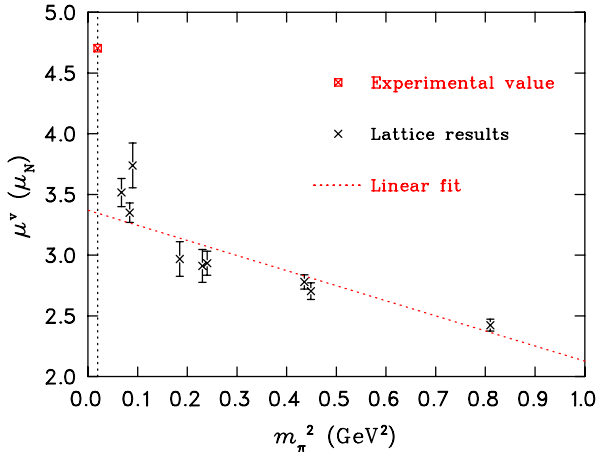

FIG. 1 (color online). Lattice QCD data for μ_N^v from QCDSF [10], with experimental value as marked [41,42]. The lattice results satisfy $L > 1.5$ fm, $m_\pi L > 3$. A simple linear fit is also included, which misses the experimental value.

$$\langle B(p') \mid J_\mu \mid B(p)\rangle = \bar{u}^{s'}(p')\Big\{\gamma_\mu F_1(Q^2) + \frac{i\sigma_{\mu\nu}q^\nu}{2m_B}F_2(Q^2)\Big\}u^s(p). \quad (1)$$

Q^2 is a positive momentum transfer $Q^2 = -(p' - p)^2$. The Sachs electromagnetic form factors G_E, M are the linear combinations of F_1 and F_2 defined by

$$G_E(Q^2) = F_1(Q^2) - \frac{Q^2}{4m_B^2}F_2(Q^2), \quad (2)$$

$$G_M(Q^2) = F_1(Q^2) + F_2(Q^2). \quad (3)$$

The Sachs magnetic form factor of the nucleon at zero-momentum transfer, $G_M(Q^2 = 0)$, defines the magnetic moment as two separate terms: the Dirac moment (unity), plus an anomalous contribution associated with the internal structure of the hadron.

$$\mu_N^v = G_M^v(Q^2 = 0) \quad (4)$$

$$= 1 + \kappa_n. \quad (5)$$

For the leading-order contributions to the magnetic moment, the standard first-order interaction Lagrangian from heavy-baryon chiral perturbation theory (χPT) is used [21–26]:

$$\mathcal{L}^{(1)}_{\chi\mathrm{PT}} = 2D\mathrm{Tr}[\bar{B}_v S_v^\mu \{A_\mu, B_v\}] + 2F\mathrm{Tr}[\bar{B}_v S_v^\mu [A_\mu, B_v]] + \mathcal{C}(\bar{T}_v^\mu A_\mu B_v + \bar{B}_v A_\mu T_v^\mu), \quad (6)$$

$$(S_v^\mu = \frac{i}{2}\gamma_5\sigma^{\mu\nu}v_\nu), \quad (7)$$

where the pseudo-Goldstone fields are encoded as the adjoint representation of $\mathrm{SU}(3)_L \otimes \mathrm{SU}(3)_R$, forming an axial vector combination A_μ:

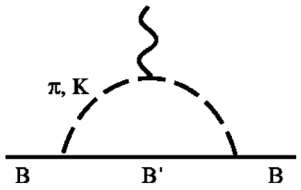

FIG. 2. The pion/kaon loop contributions to the magnetic moment of an octet baryon B, allowing a transition to a baryon B', with a photon attachment, which provides the leading nonanalytic contribution. All charge conserving transitions are implicit.

$$\xi \equiv \exp\Big\{\frac{i}{f_\pi}\tau^a\pi^a\Big\}, \quad (8)$$

$$A_\mu = \tfrac{1}{2}(\xi\partial_\mu\xi^\dagger - \xi^\dagger\partial_\mu\xi). \quad (9)$$

By the convention presented here, $f_\pi = 92.4$ MeV. The values for the couplings in the interaction Lagrangian are obtained from the SU(6) flavor-symmetry relations [23,27] and from phenomenology: $D = 0.76$, $F = \frac{2}{3}D$, and $\mathcal{C} = -2D$.

From the full Lagrangian, the chiral behavior of the magnetic moment can be written in terms of an ordered expansion in pion mass squared, through use of the Gell-Mann–Oakes–Renner relation, $m_q \propto m_\pi^2$ [28]:

$$\mu_N^v = a_0^\Lambda + a_2^\Lambda m_\pi^2 + \mathcal{T}_N(m_\pi^2;\Lambda) + \mathcal{T}_\Delta(m_\pi^2;\Lambda) + \mathcal{O}(m_\pi^4). \quad (10)$$

This expansion contains an analytic polynomial in m_π^2 plus the leading-order chiral loop integrals ($\mathcal{T}_N$, Δ), from which nonanalytic behavior arises. The coefficients a_i^Λ are the (scale-dependent) "residual series" coefficients. Upon renormalization of the divergent loop integrals, these terms correspond to low-energy coefficients of χEFT [29]. In this instance, only two free parameters are provided in the residual series. The leading-order diagrams included in this investigation are simply the 1-meson loops, as shown in Figs. 2 and 3.

A. Finite-range regularization

Finite-range regularized effective field theory handles divergences in the ultraviolet region of the loop integrals by introducing a regulator function as part of the coupling to each vertex of the diagram. The regulator function

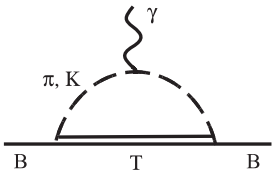

FIG. 3. The pion/kaon loop contribution to the magnetic moment of an octet baryon B, allowing transitions to nearby and strongly coupled decuplet baryons T.

$u(k;\Lambda)$ introduces a cutoff scale Λ, and should satisfy $u|_{k=0} = 1$ and $u|_{k\to\infty} = 0$. The exact functional form chosen for the regulator is independent of the result of calculation, so long as the lattice QCD results are constrained within the power-counting regime (PCR). A smooth attenuating dipole form is chosen for this investigation:

$$u(k;\Lambda) = \left(1 + \frac{k^2}{\Lambda^2}\right)^{-2}. \tag{11}$$

Detailed analyses exist for a range of alternative forms [19,30]. Though it has been suggested that a sharp cutoff FRR scheme should be chosen to ensure the preservation of the chiral Ward Identities [31], it is possible to maintain chiral symmetry by including the necessary vertex corrections at higher order in order to suppress any extra scheme-dependent nonanalytic terms induced by regulators such as the dipole [32]. Here, chiral Ward Identities are maintained to the order of the calculation.

FRR, in conjunction with χEFT-inspired techniques, provides a robust method for achieving an extrapolation to physical quark masses, and identifying an intrinsic scale embedded within lattice QCD results. It has been demonstrated previously that such an intrinsic scale may be extracted from the results of lattice QCD calculations for the mass of the nucleon [19]. This property is a consequence of the size of the PCR, defined where the expansion formulas of χPT formally hold (to finite chiral order). This extended effective field theory proceeds by analyzing the behavior of the renormalization of one or more low-energy coefficients of the chiral expansion as a function of the regularization scale. Ideally, with lattice QCD results constrained entirely within the PCR, the renormalized coefficients are independent of regularization scale. However, in practice, a scale-dependence is observed; particularly for lattice result sets including points corresponding to quark masses beyond the PCR. By truncating the lattice QCD results at different quark-mass points (corresponding to a value of $m^2_{\pi,\mathrm{max}}$), an optimal regularization scale can be identified. This optimal scale is the value at which the low-energy coefficients are least sensitive to the truncation of the lattice results [19].

B. Loop integrals and definitions

The value of the magnetic moment is renormalized by contributions from loop integrals, obtained from the effective field theory. Here, the focus is on the pion contributions, noting that it is straightforward to include the kaon contribution, using $m^2_K = m^2_{K,\mathrm{phys}} + \frac{1}{2}(m^2_\pi - m^2_{\pi,\mathrm{phys}})$, as is done in Sec. III reporting the results. The two leading-order loop integrals are the 1-meson loops, as shown in Figs. 2 and 3. Each loop integral can be expanded as a polynomial series, which is analytic in quark mass, plus a nonanalytic term:

$$\mathcal{T}_N(m^2_\pi;\Lambda) = b^N_0 + \chi_N m_\pi + b^N_2 m^2_\pi + \mathcal{O}(m^3_\pi), \tag{12}$$

$$\mathcal{T}_\Delta(m^2_\pi;\Lambda) = b^\Delta_0 + b^\Delta_2 m^2_\pi + \chi_\Delta m^2_\pi \log m_\pi/\mu + \mathcal{O}(m^3_\pi). \tag{13}$$

Here, μ is an implicit mass scale, chosen here to be 1 GeV. The coefficients of each polynomial, $b^{N,\Delta}_i$, are entirely dependent on the choice of finite-range regularization scheme, and so they are regulator-dependent quantities. The renormalization program of FRR combines the scale-dependent b_i coefficients from the chiral loops with the scale-dependent a_i coefficients from the residual series in Eq. (10) at each chiral order i, such that the result is a scale-independent coefficient c_i:

$$c_0 = a^\Lambda_0 + b^N_0 + b^\Delta_0, \tag{14}$$

$$c_2 = a^\Lambda_2 + b^N_2 + b^\Delta_2, \text{ etc.} \tag{15}$$

This means the underlying a_i coefficients undergo a renormalization from the chiral loop integrals. The renormalized coefficients c_i are an important part of the extrapolation technique. A stable and robust determination of these parameters forms the heart of determining an optimal scale Λ^{scale}.

The loop integrals can be expressed in a convenient form by taking the nonrelativistic limit and performing the pole integration for k_0. Renormalization is achieved by subtracting the relevant b^Λ_0 term from the integral, effectively absorbing it into the corresponding renormalized coefficient c_0. The integrals take the form [26,33]

$$\tilde{\mathcal{T}}_N(m^2_\pi;\Lambda) = \frac{-\chi_N}{3\pi^2}\int d^3k \frac{k^2 u^2(k;\Lambda)}{(k^2 + m^2_\pi)^2} - b^N_0, \tag{16}$$

$$\tilde{\mathcal{T}}_\Delta(m^2_\pi;\Lambda) = \frac{-\chi_\Delta}{3\pi^2}\int d^3k \frac{k^2(2\omega(k)+\Delta)u^2(k;\Lambda)}{2\omega^3(k)[\omega(k)+\Delta]^2} - b^\Delta_0. \tag{17}$$

The chiral coefficients χ_N and χ_Δ are determined from interactions in the chiral Lagrangian of Eq. (6):

$$\chi^p_N = -\frac{m_N}{8\pi f^2_\pi}(D+F)^2 = -\chi^n_N, \tag{18}$$

$$\chi^p_\Delta = -\frac{m_N}{8\pi f^2_\pi}\frac{2\mathcal{C}^2}{9} = -\chi^n_\Delta. \tag{19}$$

The chiral expansion of the magnetic moment in Eq. (10) can now be written out in a form renormalized to order $\mathcal{O}(1)$:

$$\mu^{\mathrm{v}}_N = c_0 + a^\Lambda_2 m^2_\pi + \tilde{\mathcal{T}}_N(m^2_\pi;\Lambda) + \tilde{\mathcal{T}}_\Delta(m^2_\pi;\Lambda) + \mathcal{O}(m^4_\pi). \tag{20}$$

Since lattice simulations are necessarily carried out on a discrete spacetime, any extrapolations performed should take into account finite-volume effects. χEFT is ideally suited for characterizing the leading infrared effects associated with the finite volume. In order to achieve this, each of the three-dimensional integrals can be transformed to its

form on the lattice using a finite-sum of discretized momenta, see Allton *et al.* [34] for instance:

$$\int d^3k \to \frac{(2\pi)^3}{L_x L_y L_z} \sum_{k_x,k_y,k_z}. \tag{21}$$

On the finite-volume lattice, each momentum component is quantized in units of $2\pi/L$, that is $k_i = 2\pi n_i/L$ for integers n_i. Finite-volume corrections δ^{FVC} can be written simply as the difference between the finite sum and the corresponding integral. It is known that the finite-volume corrections saturate to a fixed result for large values of regularization scale [19,35]. The value $\Lambda' = 2.0$ GeV is chosen to evaluate all finite-volume corrections independently from the integral cutoff scale Λ in Eqs. (16) and (17). This method is equivalent to the more algebraic approach outlined in Ref. [36]. The finite-volume version of Eq. (20) can thus be expressed:

$$\mu_N^{\mathrm{v}} = c_0 + a_2^{\Lambda} m_\pi^2 + (\tilde{\mathcal{T}}_N(m_\pi^2;\Lambda) + \delta_N^{\mathrm{FVC}}(m_\pi^2;\Lambda')) + (\tilde{\mathcal{T}}_\Delta(m_\pi^2;\Lambda) + \delta_\Delta^{\mathrm{FVC}}(m_\pi^2;\Lambda')) + \mathcal{O}(m_\pi^4). \tag{22}$$

III. RESULTS

A. Renormalization flow analysis

In order to obtain the most robust extrapolation, an optimal regularization scale is sought. The robustness of the extrapolation is characterized by its stability against truncation of the lattice data set. That is, a similar extrapolation should be achieved regardless of the number of data points used in the fit. The optimal regularization scale Λ^{scale} may be obtained by calculating the low-energy coefficients (e.g., c_0) from Eq. (22) for a range of regulator values Λ. Since the lattice simulation results extend outside PCR, the renormalized value of the coefficients will be scale dependent. However, the analysis in Ref. [19] demonstrates that using different amounts of lattice data yields a different scale dependence. If the lattice simulation results lie close to the PCR, the scale dependence is naturally less than if a more extensive set of lattice data is used. The optimal regularization scale is the value of Λ at which the same value of c_0 (or any low-energy coefficient) is obtained regardless of the amount of lattice data used. This is the scale where the values of the low-energy coefficients correspond to the values obtained from lattice results within the PCR [19].

Consider the behavior of c_0 from Eq. (22) as a function of the regularization scale Λ. Using different upper values of $m^2_{\pi,\mathrm{max}}$, a set of renormalization flow curves may be constructed. The renormalization flow curves including up to all nine lattice results, and using a dipole regulator, are plotted on the same set of axes in Fig. 4. As more data are included in the fit, a greater degree of regulator dependence is observed. Note that there is a reasonably well-defined Λ value at which the renormalization of c_0 is least sensitive to the truncation of the data. This indicates that there exists an optimal regularization scale embedded in the lattice QCD results.

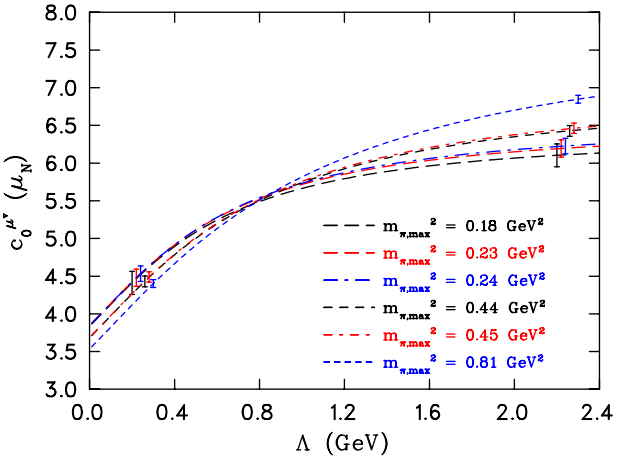

FIG. 4 (color online). The renormalization flow of c_0 for μ_N^{v} obtained using a dipole regulator on QCDSF lattice QCD results. For each curve, two arbitrary values of Λ are chosen to indicate the general size of the error bars.

The optimal regularization scale for a dipole can be extracted from Fig. 4 using a χ^2_{dof} analysis. Such an analysis will also provide a measure of the systematic uncertainty in the optimal regularization scale. By plotting χ^2_{dof} against Λ, where dof equals the number of curves n minus one, a measure of the spread of the renormalization flow curves can be calculated, and the intersection point obtained. The χ^2_{dof} is constructed at each value of Λ for c_0 (with uncertainty δc_0):

$$\chi^2_{\mathrm{dof}} = \frac{1}{n-1}\sum_{i=1}^{n}\frac{(c_0^i(\Lambda) - \bar{c}_0(\Lambda))^2}{(\delta c_0^i(\Lambda))^2}, \tag{23}$$

$$\bar{c}_0(\Lambda) = \frac{\sum_{i=1}^{n} c_0^i(\Lambda)/(\delta c_0^i(\Lambda))^2}{\sum_{j=1}^{n} 1/(\delta c_0^j(\Lambda))^2}. \tag{24}$$

The indices i and j correspond to data sets with different values of $m^2_{\pi,\mathrm{max}}$. The χ^2_{dof} plot corresponding to Fig. 4 is shown in Fig. 5. The upper and lower bounds on Λ obey the condition $\chi^2_{\mathrm{dof}} < \chi^2_{\mathrm{dof,min}} + 1/(\mathrm{dof})$. Thus, the optimal regularization scale for a dipole form is $\Lambda^{\mathrm{scale}} = 0.82^{+0.14}_{-0.13}$ GeV. This value is smaller than the optimal regularization scale obtained for the nucleon mass using a dipole form [19] based on lattice QCD results from JLQCD [37], PACS-CS [38], and CP-PACS [39]. Nevertheless, the value of the optimal scale is the same order of magnitude as those calculated from the nucleon mass analyses, and previous studies of the magnetic moment [40]. In addition, it has been assumed that all available lattice results should be used in constructing the fit. This is not necessarily the case. The method described in Ref. [20] outlines a procedure for determining the optimal fit window of pion masses, as discussed in the following section.

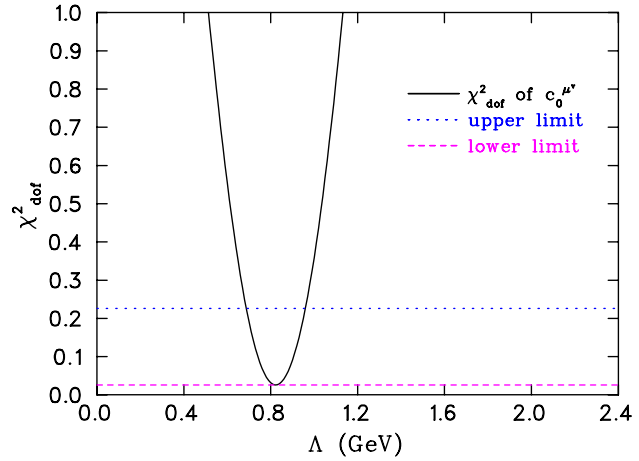

FIG. 5 (color online). $\chi^2_{\rm dof}$ for the renormalization flow of c_0 for $\mu_N^{\rm v}$ obtained using a dipole regulator on QCDSF lattice QCD results, up to and including $m^2_{\pi,\rm max} = 0.81$ GeV^2.

B. Chiral extrapolations

Using the optimal regularization scale, extrapolations can be made on various lattice volumes. In order to determine the most suitable number of data points to be used for fitting the lattice results, one may perform several extrapolations, using a varying number of points each time, and compare the size of the statistical and systematic error estimates. The statistical uncertainty comprises contributions from the fit coefficients, and the optimal regularization scale $\Lambda^{\rm scale}$, which is assumed to be independent of the other fit coefficients, and its contribution is added in quadrature. The axial coupling g_A and the pion decay constant f_π are assumed to be sufficiently well determined experimentally. The systematic uncertainty in the extrapolation is estimated by comparing the results from different regulator functional forms. The triple-dipole regulator introduced in Refs. [19,20] is considered, which interpolates between the dipole and the sharp cutoff regulators. The resultant chiral extrapolation using a dipole regulator is compared to that using a triple-dipole regulator in order to estimate the systematic uncertainty.

The quadrature sum of the statistical and systematic uncertainties in the extrapolation of $\mu_N^{\rm v}$ to the physical point, for different values of $m^2_{\pi,\rm max}$, is shown in Fig. 6. Ideally, one should find a best value of the upper limit $m^2_{\pi,\rm max}$, as indicated by the best compromise between statistical and systematic effects. Figure 6 indicates that the smallest error bar occurs when all nine lattice points are included. This set corresponds to a maximum pion-mass value: $m^2_{\pi,\rm max} = 0.81$ GeV^2. However, it is helpful to know the relative contributions from statistical and systematic sources. Table I summarizes the breakdown of each error bar into its sources. Figure 7 shows the magnitude of the

TABLE I. Results for the isovector nucleon magnetic moment for different values of $m^2_{\pi,\rm max}$, extrapolated to the physical point, corresponding to Fig. 6. The uncertainty in $\mu_N^{\rm v}(m^2_{\pi,\rm phys})$ is provided in the following order: the statistical uncertainty, the optimal regularization scale $\Lambda^{\rm scale}$, and the systematic uncertainty due to the regulator functional form, respectively.

$m^2_{\pi,\rm max}$(GeV^2)	$\mu_N^{\rm v}(m^2_{\pi,\rm phys})(\mu_N)$
0.185	4.35(13)(57)(17)
0.230	3.79(10)(60)(33)
0.240	3.79(9)(61)(32)
0.436	4.29(7)(34)(40)
0.449	4.29(7)(29)(40)
0.810	4.26(5)(16)(39)

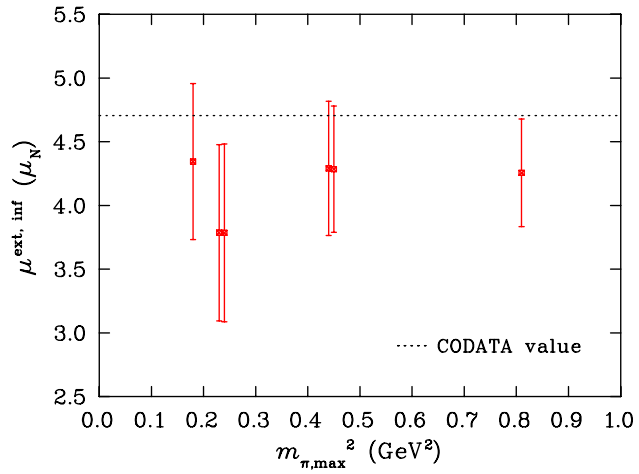

FIG. 6 (color online). Behavior of the extrapolation of $\mu_N^{\rm v}$ to the physical point vs $m^2_{\pi,\rm max}$. In each case, the value of $\Lambda^{\rm scale}$ is used, as obtained from the corresponding $\chi^2_{\rm dof}$ analysis. The error bars include the statistical and systematic uncertainties added in quadrature.

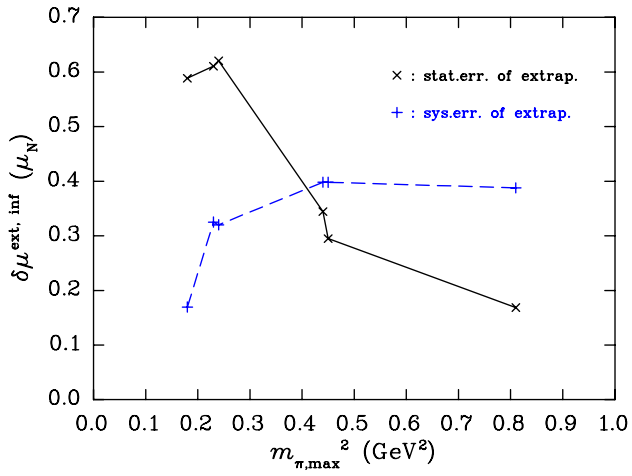

FIG. 7 (color online). Magnitude of the statistical and systematic error bar in the extrapolation of $\mu_N^{\rm v}$ to the physical point vs $m^2_{\pi,\rm max}$. In each case, the value of $\Lambda^{\rm scale}$ is used, as obtained from the corresponding $\chi^2_{\rm dof}$ analysis. At a maximum pion mass of $\bar{m}^2 = m^2_{\pi,\rm max} = 0.44$ GeV^2, the best compromise between statistical and systematic uncertainty is achieved.

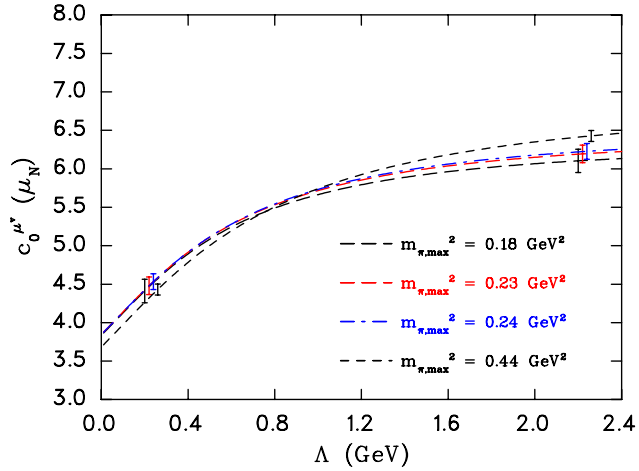

FIG. 8 (color online). The renormalization flow of c_0 for μ_N^v obtained using a dipole regulator on QCDSF lattice QCD results. Only the lightest seven lattice results are used. For each curve, two arbitrary values of Λ are chosen to indicate the general size of the error bars.

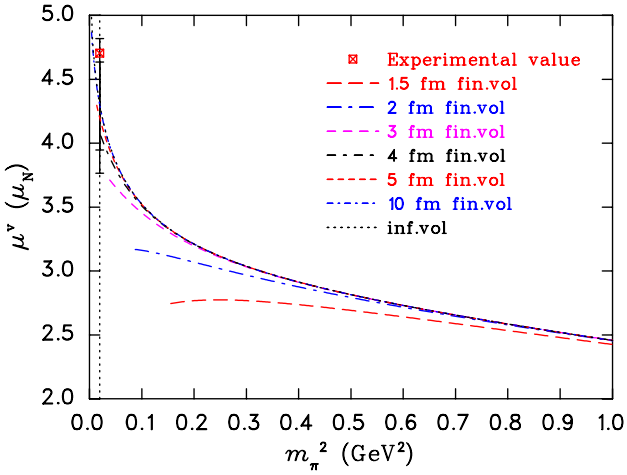

FIG. 10 (color online). Extrapolations of μ_N^v at different finite volumes and infinite volume. The curves are based on lattice QCD results from QCDSF, lattice sizes: 1.7–2.9 fm. The experimental value is marked [41,42]. In all finite-volume extrapolations, the provisional constraint $m_\pi L > 3$ is used.

statistical and systematic error bars for different values of $m^2_{\pi,\max}$. Clearly, the general trend of the statistical error bar decreases as more lattice results are considered, and likewise the general trend of the systematic error bar increases. At $m^2_{\pi,\max} = 0.44$ GeV^2, the statistical and systematic error bars are closest in magnitude, which indicates the proximity of a "sweet spot" (denoted $m^2_{\pi,\max} = \bar{m}^2$), at which the best trade-off between statistical and systematic uncertainty is achieved.

The renormalization flow curves corresponding at most to a value of $m^2_{\pi,\max} = 0.44$ GeV^2 are shown in Fig. 8, and the corresponding χ^2_{dof} plot is shown in Fig. 9. Clearly, the statistical contribution to the uncertainty in the extrapolation is larger than in the case where all lattice results are used. This is reflected in the larger uncertainty in the identification of the optimal regularization scale (at optimal $m^2_{\pi,\max} = \bar{m}^2$: $\Lambda^{\text{scale}}_{\bar{m}^2} = 0.87^{+0.42}_{-0.36}$. This value is consistent with the optimal regularization scale obtained for the nucleon mass, using a dipole form [19]. This provides evidence for the successful extraction of the intrinsic scale in the nucleon-pion interaction. Since this value of $\Lambda^{\text{scale}}_{\bar{m}^2}$ is obtained from the best compromise between statistical and systematic uncertainty, it will be used in the following chiral extrapolation of the isovector nucleon magnetic moment. Only the lightest seven lattice points (corresponding to $m^2_{\pi,\max} = 0.44$ GeV^2) will be used in the fit.

Consider the behavior of the magnetic moment as a function of the quark mass. Extrapolation curves

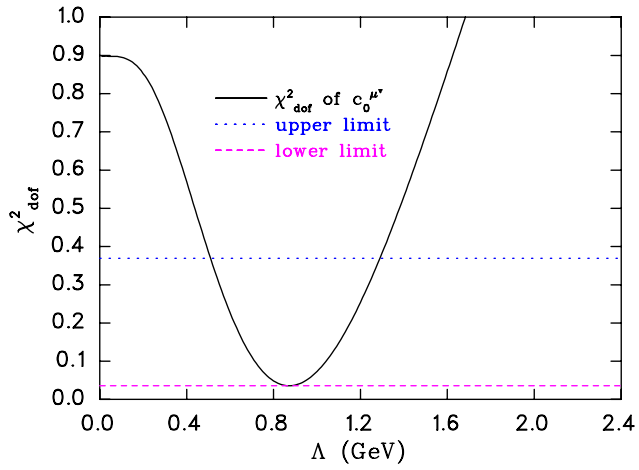

FIG. 9 (color online). χ^2_{dof} for the renormalization flow of c_0 for μ_N^v obtained using a dipole regulator on QCDSF lattice QCD results, up to and including $m^2_{\pi,\max} = 0.44$ GeV^2 only.

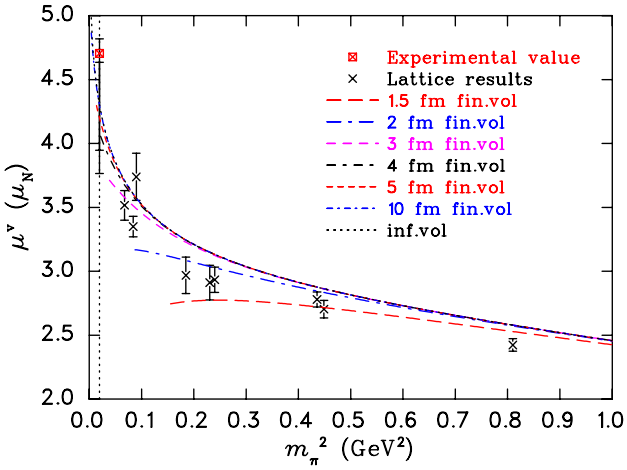

FIG. 11 (color online). Extrapolations of μ_N^v at different finite volumes and infinite volume. The finite-volume lattice QCD results from Ref. [10] are plotted for comparison, with box sizes in the range 1.7–2.9 fm. In all finite-volume extrapolations, the provisional constraint $m_\pi L > 3$ is used.

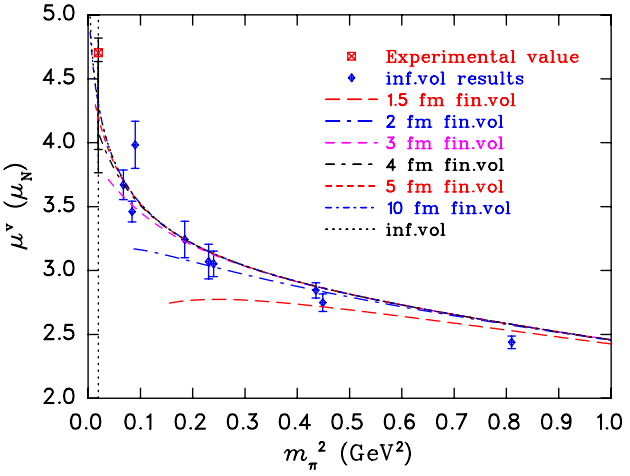

FIG. 12 (color online). Extrapolations of μ_N^v at different finite volumes and infinite volume. The lattice QCD results displayed have been corrected to infinite volume. Only the lightest seven points are used in the fit, corresponding to a value of $m^2_{\pi,\max} = 0.44$ GeV^2.

corresponding to infinite volume, and a variety of finite volumes are shown in Fig. 10. For each curve, only the values for which $m_\pi L > 3$ are plotted. These finite volumes include typical values at which current lattice QCD results are produced. For example, a full QCD simulation at physical quark masses on a (4 fm)^3 volume will significantly underestimate the infinite-volume result. These curves indicate that a box length of $L > 5$ fm is required to achieve an extrapolation within 2% of the infinite-volume result.

The finite-volume expansion of Eq. (22) is constrained by the lattice simulation results from several different volumes in the range 1.7–2.9 fm, as shown in Fig. 11. The infinite-volume extrapolation is fit to the lattice simulation results only after the results have been corrected to infinite volume. These points are shown in Fig. 12. The extrapolation to the physical point also includes an inner error bar representing only the statistical uncertainty, and an outer error bar, which also includes the systematic uncertainty due to the regulator in quadrature.

In all extrapolations, the strange quark loops have been unquenched, and the effects of kaons loops that would occur in an SU(3) lattice calculation are estimated. The result is a change of only $\approx 0.7\%$ larger at the physical point when kaons loops are included.

The finite-volume extrapolations of Fig. 10 are generally useful for estimating the result of a lattice QCD calculation at certain box sizes. This can also provide a benchmark for estimating the outcome of a lattice QCD simulation at larger and untested box sizes.

IV. CONCLUSION

The technique for obtaining an optimal regularization scale from lattice QCD results has been investigated in the context of the magnetic moment of the isovector nucleon, using recent precision lattice QCD results from QCDSF. An optimal regularization scale was identified by analyzing the renormalization flow of the low-energy coefficient c_0 with respect to the scale Λ, while extending beyond the power-counting regime. An optimal value of $m^2_{\pi,\max}$ was also obtained, where the statistical and systematic error estimates of a chiral extrapolation are comparable in magnitude. This value $\bar{m}^2$ provides a guide to the range of pion masses in which finite-range regularization techniques are not the dominant source of uncertainty in a chiral extrapolation.

A regularization scale $\Lambda^{\text{scale}}_{\bar{m}^2}$ was determined where the renormalization of c_0 is least sensitive to the truncation of the lattice QCD results. The value of the optimal regularization scale was consistent with results from the nucleon mass analysis. Thus, an intrinsic scale has been uncovered, which characterizes the energy scale of the nucleon-pion interaction. The result therefore further demonstrates the success of the procedure for using lattice QCD results to extrapolate an observable to the low-energy region of QCD.

Using the value of the intrinsic scale, the extrapolation of the magnetic moment to the physical pion mass and infinite-volume lattice box size is consistent with the experimental value. More importantly, the finite-volume extrapolations provide a benchmark for estimating the outcome of a lattice QCD simulation at realistic or optimistic lattice sizes. This serves to emphasize the importance of achieving large volumes in realizing the correct nonanalytic behavior found in nature.

ACKNOWLEDGMENTS

We would like the thank James Zanotti for many helpful discussions. This research is supported by the Australian Research Council.

[1] J. Arrington, K. de Jager, and C. F. Perdrisat, J. Phys. Conf. Ser. **299**, 012002 (2011).
[2] C. Perdrisat, V. Punjabi, and M. Vanderhaeghen, Prog. Part. Nucl. Phys. **59**, 694 (2007).
[3] J. Arrington, C. Roberts, and J. Zanotti, J. Phys. G **34**, S23 (2007).
[4] C. E. Hyde and K. de Jager, Annu. Rev. Nucl. Part. Sci. **54**, 217 (2004).

[5] H.-y. Gao, Int. J. Mod. Phys. E **12**, 1 (2003).
[6] T. Yamazaki, Y. Aoki, T. Blum, H.-W. Lin, S. Ohta, S. Sasaki, R. Tweedie, and J. Zanotti, Phys. Rev. D **79**, 114505 (2009).
[7] S. Syritsyn, J. Bratt, M. Lin, H. Meyer, J. Negele *et al.*, Phys. Rev. D **81**, 034507 (2010).
[8] J. Bratt *et al.* (LHPC Collaboration), Phys. Rev. D **82**, 094502 (2010).
[9] C. Alexandrou, M. Brinet, J. Carbonell, M. Constantinou, P. Harraud, P. Guichon, K. Jansen, T. Korzec, and M. Papinutto, Phys. Rev. D **83**, 094502 (2011).
[10] S. Collins, M. Gockeler, P. Hagler, R. Horsley, Y. Nakamura *et al.*, Phys. Rev. D **84**, 074507 (2011).
[11] D. B. Leinweber, R. Woloshyn, and T. Draper, Phys. Rev. D **43**, 1659 (1991).
[12] V. Bernard, N. Kaiser, J. Kambor, and U. G. Meissner, Nucl. Phys. **B388**, 315 (1992).
[13] T. R. Hemmert and W. Weise, Eur. Phys. J. A **15**, 487 (2002).
[14] M. Dorati, T. A. Gail, and T. R. Hemmert, Nucl. Phys. **A798**, 96 (2008).
[15] M. Göckeler, T. R. Hemmert, R. Horsley, D. Pleiter, P. E. L. Rakow, A. Schäfer, and G. Schierholz, (QCDSF), Phys. Rev. D **71**, 034508 (2005).
[16] S. Boinepalli, D. B. Leinweber, A. G. Williams, J. M. Zanotti, and J. B. Zhang, Phys. Rev. D **74**, 093005 (2006).
[17] D. B. Leinweber, A. W. Thomas, and R. D. Young, Phys. Rev. Lett. **92**, 242002 (2004).
[18] R. D. Young, D. B. Leinweber, and A. W. Thomas, Phys. Rev. D **71**, 014001 (2005).
[19] J. M. M. Hall, D. B. Leinweber, and R. D. Young, Phys. Rev. D **82**, 034010 (2010).
[20] J. M. M. Hall, F. X. Lee, D. B. Leinweber, K. F. Liu, N. Mathur, R. D. Young, and J. B. Zhang, Phys. Rev. D **84**, 114011 (2011).
[21] E. E. Jenkins and A. V. Manohar, in Workshop on Effective Field Theories of the Standard Model, Dobogoko, Hungary, 1991 (unpublished).
[22] E. E. Jenkins and A. V. Manohar, Phys. Lett. B **255**, 558 (1991).
[23] E. E. Jenkins, Nucl. Phys. **B368**, 190 (1992).
[24] J. N. Labrenz and S. R. Sharpe, Phys. Rev. D **54**, 4595 (1996).
[25] A. Walker-Loud, Nucl. Phys. **A747**, 476 (2005).
[26] P. Wang, D. B. Leinweber, A. W. Thomas, and R. D. Young, Phys. Rev. D **75**, 073012 (2007).
[27] R. F. Lebed, Phys. Rev. D **51**, 5039 (1995).
[28] M. Gell-Mann, R. J. Oakes, and B. Renner, Phys. Rev. **175**, 2195 (1968).
[29] R. D. Young, D. B. Leinweber, and A. W. Thomas, Prog. Part. Nucl. Phys. **50**, 399 (2003).
[30] D. B. Leinweber, A. W. Thomas, and R. D. Young, Nucl. Phys. **A755**, 59 (2005).
[31] V. Bernard, T. R. Hemmert, and U.-G. Meissner, Nucl. Phys. **A732**, 149 (2004).
[32] D. Djukanovic, M. R. Schindler, J. Gegelia, and S. Scherer, Phys. Rev. D **72**, 045002 (2005).
[33] P. Wang, D. B. Leinweber, A. W. Thomas, and R. D. Young, Phys. Rev. D **79**, 094001 (2009).
[34] W. Armour, C. R. Allton, D. B. Leinweber, A. W. Thomas, and R. D. Young, J. Phys. G **32**, 971 (2006).
[35] A. Ali Khan *et al.* (QCDSF-UKQCD), Nucl. Phys. **B689**, 175 (2004).
[36] S. R. Beane, Phys. Rev. D **70**, 034507 (2004).
[37] H. Ohki, H. Fukaya, S. Hashimoto, T. Kaneko, H. Matsufuru, J. Noaki, T. Onogi, E. Shintani, and N. Yamada, Phys. Rev. D **78**, 054502 (2008).
[38] S. Aoki *et al.* (PACS-CS), Phys. Rev. D **79**, 034503 (2009).
[39] A. Ali Khan *et al.* (CP-PACS), Phys. Rev. D **65**, 054505 (2002).
[40] D. B. Leinweber, D. H. Lu, and A. W. Thomas, Phys. Rev. D **60**, 034014 (1999).
[41] P. J. Mohr, B. N. Taylor, and D. B. Newell, Rev. Mod. Phys. **80**, 633 (2008).
[42] K. Nakamura *et al.* (Particle Data Group), J. Phys. G **37**, 075021 (2010).